View metadata, citation and similar papers at core.ac.uk

brought to you by CORE

provided by Elsevier - Publisher Connector

Weather and Climate Extremes 4 (2014) 62–74

Contents lists available at ScienceDirect

Weather and Climate Extremes

journal homepage: www.elsevier.com/locate/wace

Mechanism of early-summer low-temperature extremes in Japan projected by a nonhydrostatic regional climate model

Akihiko Murata *, Hidetaka Sasaki, Mizuki Hanafusa, Kazuo Kurihara

Meteorological Research Institute, Tsukuba, Ibaraki 305-0052, Japan

ARTICLE INFO

Article history:
Received 22 August 2013
Received in revised form
17 April 2014
Accepted 19 April 2014
Available online 30 April 2014

Keywords:
Extreme
Temperature
Regional
Climate
Model

ABSTRACT

We investigated the mechanisms associated with projected early-summer low-temperature extremes in Japan at the end of the 21st century by means of a well-developed nonhydrostatic regional climate model under the A1B scenario provided by the Intergovernmental Panel on Climate Change-Special Report on Emission Scenario. The projected surface air temperature reveals that even in a climate warmer than that at present, extremely low daily minimum temperatures in early summer are comparable to those in the present climate at several locations. At locations where future low temperatures are remarkable, the temperature drop at night is larger in the future than at present. This temperature drop results from mainly two heat fluxes: upward longwave radiation and latent heat flux. In the future climate, upward longwave radiation increases owing to high temperature at the surface around the time of the sunset. In addition, the upward flux of latent heat increases owing to low relative humidity just above the surface. These dryer conditions are associated with lower relative humidity at 850 hPa, suggesting the effects of synoptic systems. These two fluxes act to reduce the surface temperature, and hence surface air temperature.

© 2014 The Authors. Published by Elsevier B.V. This is an open access article under the CC BY-NC-ND license (http://creativecommons.org/licenses/by-nc-nd/3.0/).

1. Introduction

Temperature change is one of the central issues surrounding future projections of the climate. Projections of future temperature associated with anthropogenic global warming are important for every branch of human activities and natural systems: human health, ecosystems, and a variety of industries, such as agriculture, energy, and insurance.

Although climate warming projections usually present mean temperature increases, recently, extreme temperatures have been projected because human activities will be significantly affected not only by changes in mean temperatures, but also changes in extreme temperatures. Global warming might induce regional- or local-scale temperature extremes. According to (Anderson (2011, 2012), even with an increase in the global-mean temperature of only 2 K, broad areas of the globe could experience maximum seasonal-mean temperatures exceeding historical extremes. Projections of extreme temperatures on regional scales are needed; to achieve this, we need regional climate models (RCM) that capture finer-scale changes in temperature over space and time (e.g., Kurihara et al., 2005; Rummukainen, 2010; Arritt and Rummukainen, 2011).

Previous studies at regional scales primarily focused on higher temperature extremes such as changes to the daily maximum temperature in summer; for example, using the simulation projected by the A1B scenario provided by the Intergovernmental Panel on Climate Change (IPCC) Special Report on Emission Scenario (SRES) (IPCC, 2000), Murata et al. (2012) examined future changes in summertime temperature extremes over Japan projected by an RCM with a high spatial resolution of 5 km. Projected changes in extreme daily maximum and minimum temperatures were relatively large over several areas leeward of mountains. Using two state-of-the-art RCMs, Frías et al. (2012) found that in the future climate under the A1B scenario during spring and summer in Southern Europe, the extremes are two or three times the increases in mean seasonal temperatures. Rangwala et al. (2012) projected temperature extremes in mid-21st century in the southern Colorado Rocky Mountains by using RCMs under the A2 scenario provided by the IPCC-SRES; at higher elevations mean daily maximum temperature during summer increases more than 3 K in addition to increases of around 2 K for all seasons.

In addition to high temperature extremes, projections of future low temperature extremes are also important because many human activities are vulnerable to cold extremes, regardless of overall climate warming. For example, some crops are vulnerable to extremely low temperatures. Luo (2011) reviewed temperature thresholds for a variety of crops to provide a basis for estimating the probability of exceeding temperature thresholds. Among these

* Corresponding author. Tel.: +81 29 853 8732.
E-mail address: amurata@mri-jma.go.jp (A. Murata).

http://dx.doi.org/10.1016/j.wace.2014.04.007
2212-0947/© 2014 The Authors. Published by Elsevier B.V. This is an open access article under the CC BY-NC-ND license (http://creativecommons.org/licenses/by-nc-nd/3.0/).

thresholds, base temperature and lethal minimum temperature were defined: the former is the temperatures below which grain yield fails to zero and the latter is the temperature below which recovery of function is impossible. Other human activities and natural systems vulnerable to cold extremes have also been examined, such as human health (Patz et al., 2005; Handmer et al., 2012) and ecosystems (Handmer et al., 2012; Inouye, 2000).

Few studies have investigated the changes to low-temperature extremes associated with global warming, although such extreme events may significantly impact human activities. Kodra et al. (2011) is a rare example; they analyzed projections provided by GCMs and found that cold extremes could persist even under 21st-century warming scenarios. Their results indicate that in many regions of the globe, the intensity and duration of cold extremes would be comparable to those under current typical conditions. Park et al. (2011) examined the changes to cold extreme events over East Asia by using projections provided by GCMs. The projections showed frequent occurrences of cold surges even in the future climate; these surges are comparable to those in the present climate, and Park et al. pointed out that living things in the future climate would suffer the impact of cold surges. Their results were primarily focused on synoptic-scale systems and indicate that the minor changes to the frequency of cold surges are due to the nearly constant magnitude of the Siberian High during the time between the present and future. However, local-scale effects on cold extreme events were not investigated in these previous studies because local-scale phenomena are not adequately resolved by GCMs.

No studies have, so far, investigated local- or regional-scale low-temperature extremes across Japan under global warming conditions although such extremes may severely impact human activities in Japan. Because Japan has complex topography and coastlines, which lead to considerable climate variability, the necessary projections of low-temperature extremes should be prepared at fine spatial scales (local or regional). To capture low-temperature extremes at the local- or regional-scale, it will be necessary to use a high-resolution RCM with grids fine enough to capture such small spatial and temporal variations. Recently, a high-resolution nonhydrostatic RCM (called NHRCM), developed from a nonhydrostatic mesoscale model, has been used to simulate regional climates in Japan (e.g., Murata et al., 2012; Sasaki et al., 2008; Kanada et al., 2008; Nakano et al., 2012; Bai et al., 2013). In particular, Sasaki et al. (2011, 2012) conducted high-resolution regional climate simulations for all seasons in Japan and reported on the superior performance of the NHRCM over that of a GCM. Using this dataset, several studies of regional climates in Japan were conducted (Sasaki et al., 2013; Hanafusa et al., 2013; Murata et al., 2013).

In this study, we used data obtained from NHRCM simulations to perform a detailed assessment of local-scale low-temperature extremes in Japan under the future climate; we found extremely low temperatures in early summer. Therefore, our focus is on low-temperature extremes in early summer, when suitable conditions are crucial for a variety of crops because early summer corresponds to the growing season.

The aim of this study was to estimate future changes in local-scale low-temperature extremes in early summer across Japan by means of a well-developed high-resolution RCM (i.e., NHRCM) and to identify possible factors that control such changes. To do this, we explored the mechanisms for projected low-temperature extremes by using budget analysis of heat fluxes at the ground surface, which are linked to surface air temperature. Few studies have investigated local-scale heat budgets in projected future climate.

Section 2 describes the data and the methods for numerical simulations obtained with the NHRCM. Section 3 evaluates the performance of the NHRCM with respect to low-temperature extremes in the present climate. Section 4 investigates the simulated data on low-temperature extremes in the future climate. Section 5 identifies the atmospheric situations that give rise to extremely low temperatures and examines the key factors that govern the occurrence of low-temperature extremes. Section 6 assesses uncertainties in projected low-temperature extremes by employing the bootstrapping approach. Finally, section 7 presents the discussion and conclusions.

2. Data and methods

2.1. Data

2.1.1. Model data

The NHRCM developed by Sasaki et al. (2008) is a climate extension of the Japan Meteorological Agency Nonhydrostatic Model (JMA-NHM) (Saito et al., 2006, 2007), which is one of the numerical weather-prediction models operated by the JMA. The NHRCM has fully compressible equations with a map factor and uses a semi-implicit time integration scheme. It includes the bulk-type cloud microphysics (Ikawa et al., 1991; Lin et al., 1983; Murakami 1990; Murakami et al., 1994). The Kain–Fritsch convection scheme (Kain and Fritsch 1990; Kain 2004; Kato et al., 2010) is included as a cumulus scheme. For a planetary boundary layer scheme, the Mellor–Yamada–Nakanishi–Niino Level 3 scheme (Nakanishi and Niino, 2004) is employed. For radiation, a clear-sky radiation scheme (Yabu et al., 2005) and a cloud radiation scheme (Kitagawa, 2000) are used. The land-surface scheme by Hirai and Oh'izumi (2004), improved from the simple biosphere model (Sellers et al., 1986), is included. Land-cover classification is derived from the global land-cover characterization for the simple biosphere model from the U.S. Geological Survey land-use classification. Surface air temperature (1.5 m height) is diagnosed from the surface skin temperature and the temperature of the lowest atmospheric layer, based on the Monin–Obukhov similarity theory (Beljaars and Holtslag, 1991).

For long-term climate simulation, the NHRCM includes a spectral boundary coupling scheme (Kida et al., 1991; Sasaki et al., 2000). In this scheme, large-scale components produced by the outer model are merged into smaller-scale components in the inner model. Consequently, no contradiction in the large-scale components exists between the inner and outer models, thereby enabling us to integrate the inner model steadily for a long period.

The NHRCM has been used successfully to simulate regional climates in Japan. For example, Sasaki et al. (2011), using the NHRCM with 5 km grid spacing, performed a 20-year integration with predicted boundary conditions and demonstrated that the annual mean surface air temperature and precipitation in the present climate are reproduced well. Sasaki et al. (2012) performed a 20-year integration (from 2076 to 2096) for the end of the 21st century and showed a 3 K rise in surface air temperature averaged over Japan for each month (99% confidence level), compared with the temperature in the present (from 1980 to 2000). Using data obtained from Sasaki et al. (2011), Murata et al. (2013) pointed out negative biases in daily mean, maximum, and minimum temperatures in urban areas; they demonstrated that these biases are useful for estimating urban heat island intensity.

Data obtained from Sasaki et al. (2011, 2012) are utilized in this study. The grid-nesting strategy for numerical simulations is as follows. The model domain (211×661 grid points) of the NHRCM with a grid spacing of 5 km (NHRCM05) is set to cover Japan. Boundary conditions for the NHRCM05 are derived from a

simulation obtained via the NHRCM with a grid spacing of 15 km (NHRCM15) and a domain (229 × 217 grid points) that covers East Asia. The vertical coordinate of the NHRCM is terrain-following and contains 40 levels, with the lowest level located 20 m above the ground surface and the highest level located at 21.9 km. Boundary conditions for the NHRCM15 are derived from a simulation obtained with an atmospheric general circulation model (AGCM) with 20 km horizontal resolution (MRI-AGCM3.2S, hereinafter referred to as the AGCM20) (Mizuta et al., 2012). Since AGCM20 does not contain mixing ratios of cloud condensate and precipitating hydrometeors, the NHRCM15 is nested between the NHRCM05 and the AGCM20 to provide the mixing ratio to the lateral boundary for the NHRCM05 (see Sasaki et al. (2011) and Murata et al. (2013) for more details of the nesting strategy).

The AGCM20 was jointly developed by JMA and the Meteorological Research Institute of Japan; it is based on a numerical weather-prediction model operated by JMA, with several modifications of radiation and land-surface processes for use in climate simulations. The simulations are performed at a spectral triangular truncation of spherical function at wave number 959 with a linear grid for wave-to-grid transformation (TL959), corresponding to a horizontal resolution of 20 km (1920 × 960 transform grids). The model has 60 layers in the vertical direction (top at 0.1 hPa).

For the present climate, AGCM20 was run under the conditions given by the Atmospheric Model Intercomparison Project AGCM simulation for the 20th century experiment of the IPCC Fourth Assessment Report (AR4) (IPCC, 2007). In the simulation, monthly mean data from the Hadley Centre sea ice and sea surface temperature (SST) data set version 1 (HadISST1) (Rayner et al., 2003) were used for the observed SST and sea-ice concentration data. The monthly climatology of sea-ice thickness from Bourke and Garrett (1987) was also used. The NHRCM15 and NHRCM05 were run for 20 years, from September 1980 to August 2000. The NHRCM15 (NHRCM05) was initialized for 2 months (1 month) before the beginning of September in each year and was run through August of the following year, excluding the first 2 months (1 month) of the simulation, which was discarded as model spinup.

As for the climate at the end of the 21st century, AGCM20 was run under conditions with increased concentrations of greenhouse gases and higher SST consistent with the A1B scenario provided by the IPCC-SRES (IPCC, 2000). The SST used for the AGCM simulation is the sum of the following three components: (1) the future change in the multi-model ensemble of the SST projected by the Coupled Model Intercomparison Project (CMIP), phase 3 multi-model dataset; (2) the linear trend in the multi-model ensemble of the SST for the period of 2075–2099; and (3) the detrended observations for the SST for the period of 1979–2003. A detailed description of the experimental design for the AGCM20 is given by Kitoh et al. (2009). The NHRCM15 and NHRCM05 were run for 20 years, from September 2076 to August 2096. As in the case of the experiment for the present climate, the NHRCM15 (NHRCM05) was initialized for 2 months (1 month) before the beginning of September in each year and was run through August of the following year.

2.1.2. Observational data

The performance of the NHRCM05 was evaluated by comparing daily minimum temperature from the simulation of the present climate with observational data for the same period. High-resolution observations are desirable for assessing the NHRCM05 performance because of its fine grid spacing. For this purpose, we employed surface observational data with a high spatial resolution provided by the automated meteorological data acquisition system (AMeDAS) administered by JMA. AMeDAS is a ground-based observation system with a dense network of meteorological stations throughout Japan at an average interval of 17 km. Surface air temperature data are available at 700 of these stations. The 1-h temporal resolution of AMeDAS data is the same as that of the NHRCM05 output. For each AMeDAS station, we employed the following criteria for judging whether to use the data: records contain no missing (1-h temporal-resolution) data over a day (i.e., 24 data are required) and contain less than 50% missing daily data over 20 years for each calendar day (i.e., at least 10 years are required).

The model data corresponding to the nearest land grid point to each AMeDAS station were extracted. For each station location, there exists a height discrepancy between the model and the actual topography: the elevations used in the simulations at the station locations are generally higher than the actual elevations. Because this discrepancy in elevation contributed to the difference in surface air temperature between the simulated and observed data, the temperatures in the simulations were corrected with the standard temperature lapse rate (0.0065 K m^{-1}). Murata et al. (2013) examined the sensitivity to lapse rate and found that the results were insensitive to lapse rate.

2.2. Methods

2.2.1. Bias correction

Before assessing extremely low temperatures, we corrected the simulated temperatures on the basis of observational data to reduce errors. For this purpose, we applied a bias correction to the simulated daily mean temperature (Ta), daily maximum temperature (Tx), and daily minimum temperature (Tn). A number of methods for correcting biases have been proposed (e.g., Leander and Buishand, 2007; Hurkmans et al., 2010; Piani et al., 2010a,b; Bordoy and Burlando, 2013). We adopted the method proposed by Piani et al. (2010) (referred to as the P2010 method) because of its simplicity and the conservation of the order of temperature sequence in the future climate. That is, the relationship $T_1 < T_2$ in raw temperature is also satisfied by the corrected temperature, where T_1 and T_2 are arbitrary temperatures.

The P2010 method is described briefly. This method assumes the linear relationship of cumulative density functions in temperature between observations and model outputs. The following procedure is carried out for each station and each month. Firstly, data are listed in the order of Ta value for model outputs (x) and observations (y). Secondly, coefficients a and b of equation $y = a + bx$ are derived from the least square method. Next, $a + bx$ is regarded as the corrected value of Ta. Similarly, the range and skewness in temperature are also corrected. Finally, corrected values of the range and skewness are converted to Tx and Tn.

2.2.2. Most extreme daily minimum temperatures

As an index of extremely low temperature, we introduce the first (Tn01) and second (Tn02) percentiles of daily minimum temperature for each location and for each month. In this study, Tn01 and Tn02 in June are used because our analysis is focused on temperatures in early summer, as mentioned earlier. For the calculation of Tn01 and Tn02 in June for each location, the daily minimum temperature was first calculated from hourly data, where a day was defined based on local standard time (Japan Standard Time (JST)). Next, we sorted the daily minimum temperature using all data (the number of data points is 600 = 30 days × 20 years) and Tn01 and Tn02 were subsequently derived from the sorted data.

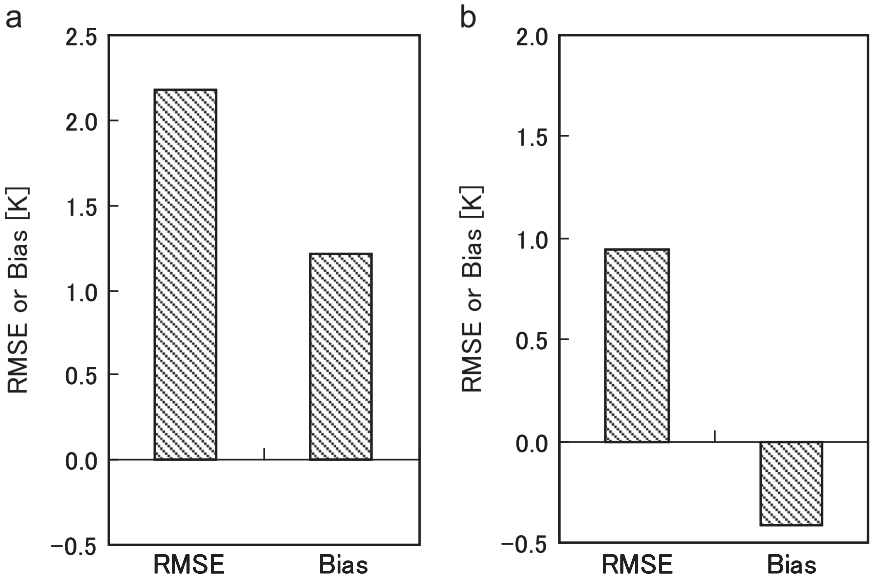

Fig. 1. Root mean square error (RMSE) and bias in the first percentile of daily minimum temperature (Tn01) in June for the present climate reproduced by the nonhydrostatic regional climate model with 5 km grid spacing (NHRCM05). RMSE and bias are shown (a) before and (b) after applying a bias correction.

3. Evaluation of low temperature in present climate

Model performance in reproducing extremely low temperature near the surface in June in the present climate was assessed by comparing the NHRCM05 simulation results with observational data for the same period from the nearest AMeDAS stations. We calculated the root mean square errors (RMSE) and the systematic errors (bias) for Tn01 in June with the following equations:

$$\mathrm{RMSE} = \sqrt{\frac{1}{N}\sum_{k=1}^{N}(M_k - O_k)^2} \quad (1)$$

$$\mathrm{bias} = \frac{1}{N}\sum_{k=1}^{N}(M_k - O_k), \quad (2)$$

where M represents simulated values, O is observed values, and N (≈ 700) is the number of AMeDAS stations for which data are available.

RMSE for Tn01 in June is approximately 2.2 K, although the bias is approximately 1.2 K (Fig. 1a), suggesting that errors for Tn01 simulated by NHRCM05 are somewhat large. Note that the RMSE and bias in the monthly mean of daily mean temperatures (i.e., Ta, Tx, and Tn) in June are within 1.5 K (not shown), comparable to those for the annual mean of the daily temperatures, which are also within 1.5 K (Murata et al., 2013), indicating that the model reproduces well the mean temperatures in the present climate in June. Because the error of 2.2 K is somewhat large, we applied the P2010 method to the simulated daily temperatures so that extremely low temperature could be reproduced more accurately.

Errors in Tn01 in June are greatly reduced by applying the P2010 method (Fig. 1b): the RMSE is approximately 1.0 K and the magnitude of bias is approximately 0.4 K, both around half those determined before applying the bias correction. In addition, the frequency distribution of the corrected Tn01 in June is in good agreement with those observed, compared with those not corrected (Fig. 2).

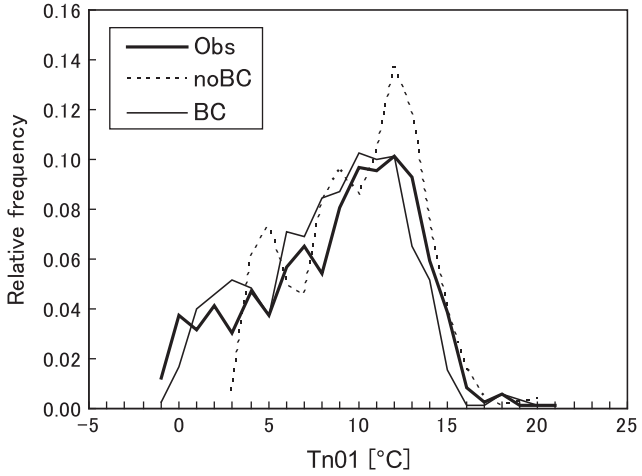

Fig. 2. Frequency distribution of Tn01 in June in the present climate for modeled (BC: bias corrected, noBC: no bias corrected) and observed (Obs) values.

4. Projection of low temperature in the future climate

We examined the spatial distribution of Tn01 and how it changes between the present and future climate (Fig. 3), where the change is defined as the difference in Tn01 between the present and future climates (future minus present). Much of our attention is focused on small changes, which means that extremely low temperatures in the future climate are comparable to those in the present climate. It should be noted that Fig. 3b only shows locations where the change in Tn01 is within 1.0 K and where the observational data are available over the whole period (i.e., 20 years) for ensuring high-quality bias correction.

There are several locations where the change in Tn01 is below 1.0 K (Fig. 3b). Among these locations, we examined physical situations at the AMeDAS station Kuma, Yusuhara, Kamioka, and Inabu, where the changes in Tn01 show 0.69, 0.97, 0.76, and 0.71 K, respectively. The station Kusatsu and Dorobe were excluded from the analysis because temperatures there were affected strong wind events owing to high altitudes (over 900 m).

The small changes in Tn01 at the locations mentioned above are robust. In order to investigate the robustness of the results obtained from a grid box corresponding to each station, changes in Tn01 at adjacent four grid boxes are also calculated. The averages of changes in Tn01 over the five grid boxes (i.e., a grid box and the adjacent four grid boxes) are 1.39, 1.41, 1.01, and 1.50 K for Kuma, Yusuhara, Kamioka, and Inabu, respectively. These values are larger than those calculated based on a grid box because of the averaging process. Nevertheless, the spatially averaged changes in

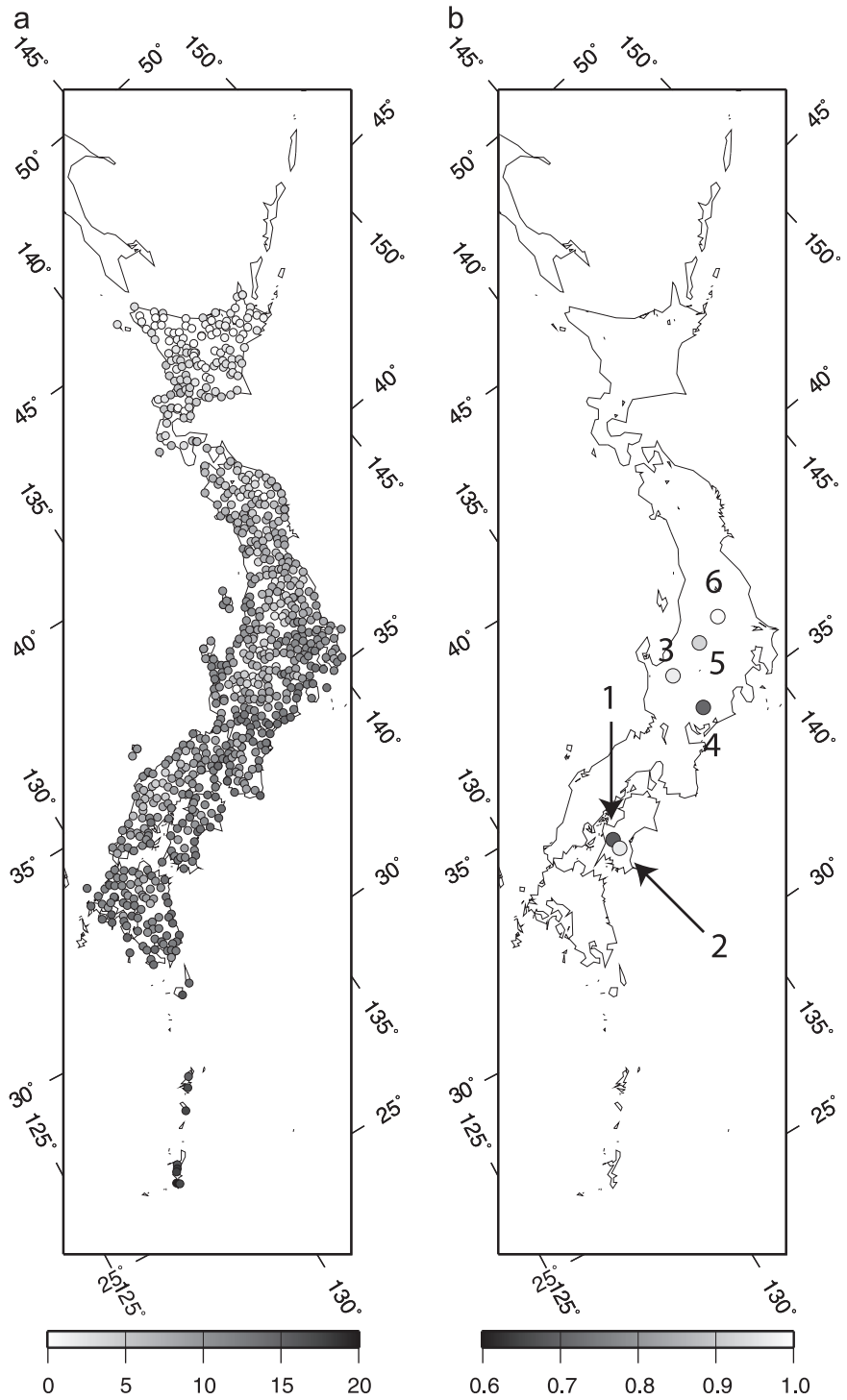

Fig. 3. Horizontal distribution of (a) Tn01 [°C] in June for the present climate simulated by the NHRCM05 and (b) the difference in Tn01 [K] in June between the present and future climates (future Tn01–present Tn01) simulated by the NHRCM05 for values < 1.0 K. The numbers on the map show the locations of (1) Kuma, (2) Yusuhara, (3) Kamioka, (4) Inabu, (5) Kusatsu and (6) Dorobe.

Tn01 are all within 1.5 K, which is much smaller compared with changes in the mean temperature (i.e., about 3 K) averaged over Japan for each month (Sasaki et al., 2012).

5. Mechanism of extremely low temperature in future climate

5.1. Temperature drop in the nighttime

We first examined the relationship between Tn and change in surface air temperature at nighttime (referred to as ΔT), which we define as the temperature just before the sunrise (at 0400 or 0500 JST depending on locations) minus that just after the sunset (at 2000 JST). Fig. 4 shows a scatterplot of ΔT and Tn. For each location, the total number of data is 600 (30 days $\times$ 20 years) for each climate. Fig. 4 reveals that, at all four locations, Tn is proportional to ΔT for each climate. The future climate shifts toward higher minimum temperatures and smaller ΔT than under the present climate. For extremely low Tn, ΔT has a negative value and the magnitude of ΔT (i.e., $|\Delta T|$) is large. For the future climate, a larger $|\Delta T|$, compared with the present climate, is necessary for the

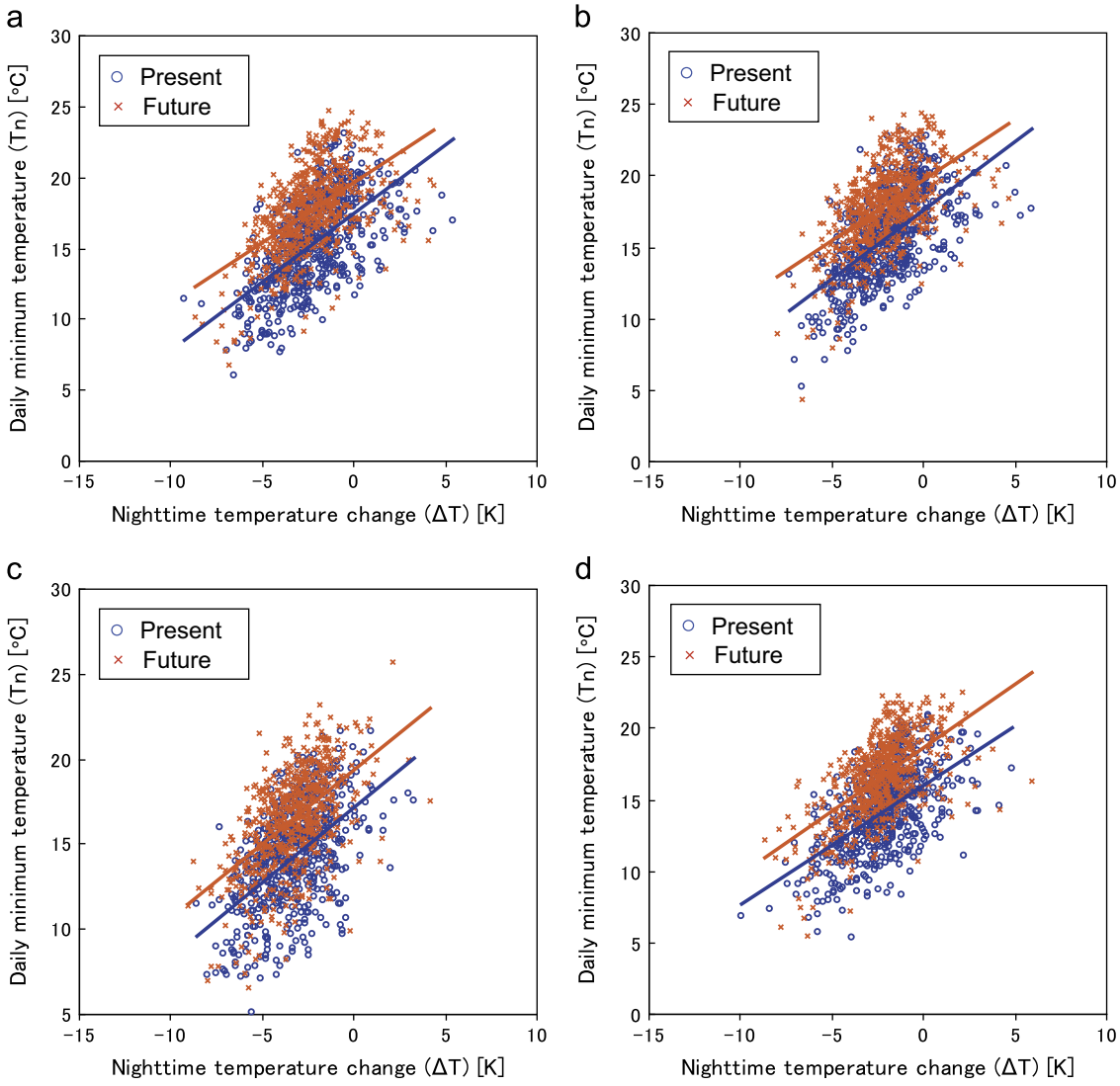

Fig. 4. Daily minimum air temperature versus the daily change in surface air temperature at nighttime (temperature just before sunrise minus that just after sunset) at (a) Kuma, (b) Yusuhara, (c) Kamioka, and (d) Inabu, in June for the present and future climate simulated by the NHRCM05. The lines are the least linear squares fits between the two quantities.

realization of extremely low temperature that is comparable to that in the present climate.

We attribute the small Tn01 at Kuma in the future climate, comparable to that in the present climate, to a relatively large $|\Delta T|$ in the future climate. Here we selected the 12 cases for each climate in which Tn is at or lower than Tn02 (Fig. 5a). The values of $|\Delta T|$ in the future climate range roughly from 6 to 9 K except for two outliers around 3 K, whereas that in the present climate ranges roughly between 4 and 7 K (Fig. 5a). Overall, in the cases of extremely low temperature, $|\Delta T|$; is larger in the future climate than in the present climate, although the Tn in the two climates is similar.

Note that the two outliers in the future climate are associated with a downward flux of sensible heat. A close inspection reveals that sensible heat contributes considerably to total heat flux and hence $|\Delta T|$ (not shown). The cases for which the downward flux of sensible heat is large correspond to those for which the surface wind speed is high (Fig. 6a), suggesting that the wind speed contributes greatly to sensible heat flux through turbulence in the planetary boundary layer. The cases for which the surface wind speed exceeds 2.2 m s^{-1} are excluded to remove the outliers (Fig. 6a). The remaining cases are calm and clear nights, with both weak surface winds and large $|\Delta T|$; in fact, longwave radiative cooling is important in these cases (not shown).

For the other three locations (i.e., Yusuhara, Kamioka, and Inabu), the relationship between Tn and ΔT is similar to that at Kuma. That is, $|\Delta T|$ is larger in the future climate than in the present climate in the cases of extremely low Tn. Fig. 5b–d shows the same scatterplots as Fig. 5a, but for the other locations. The 12 cases (at or lower than Tn02) were selected for Yusuhara, whereas the 6 cases (at or lower than Tn01) were selected for each Kamioka and Inabu. The reason for the selection of the lower threshold for Kamioka and Inabu is that the values of Tn between Tn01 and Tn02 for the future climate are not close to those for the present climate. Similar to the Kuma case, the data for which the surface wind speed exceeds 2.2 m s^{-1} are excluded to remove the outliers at Yusuhara and Inabu (Fig. 6b and d). Overall, $|\Delta T|$ is larger in the future climate than in the present climate when the data with similar Tn are compared (Fig. 5b–d).

5.2. Heat flux budget

The difference in the nighttime temperature change at Kuma for the coldest June days between the present and future climates

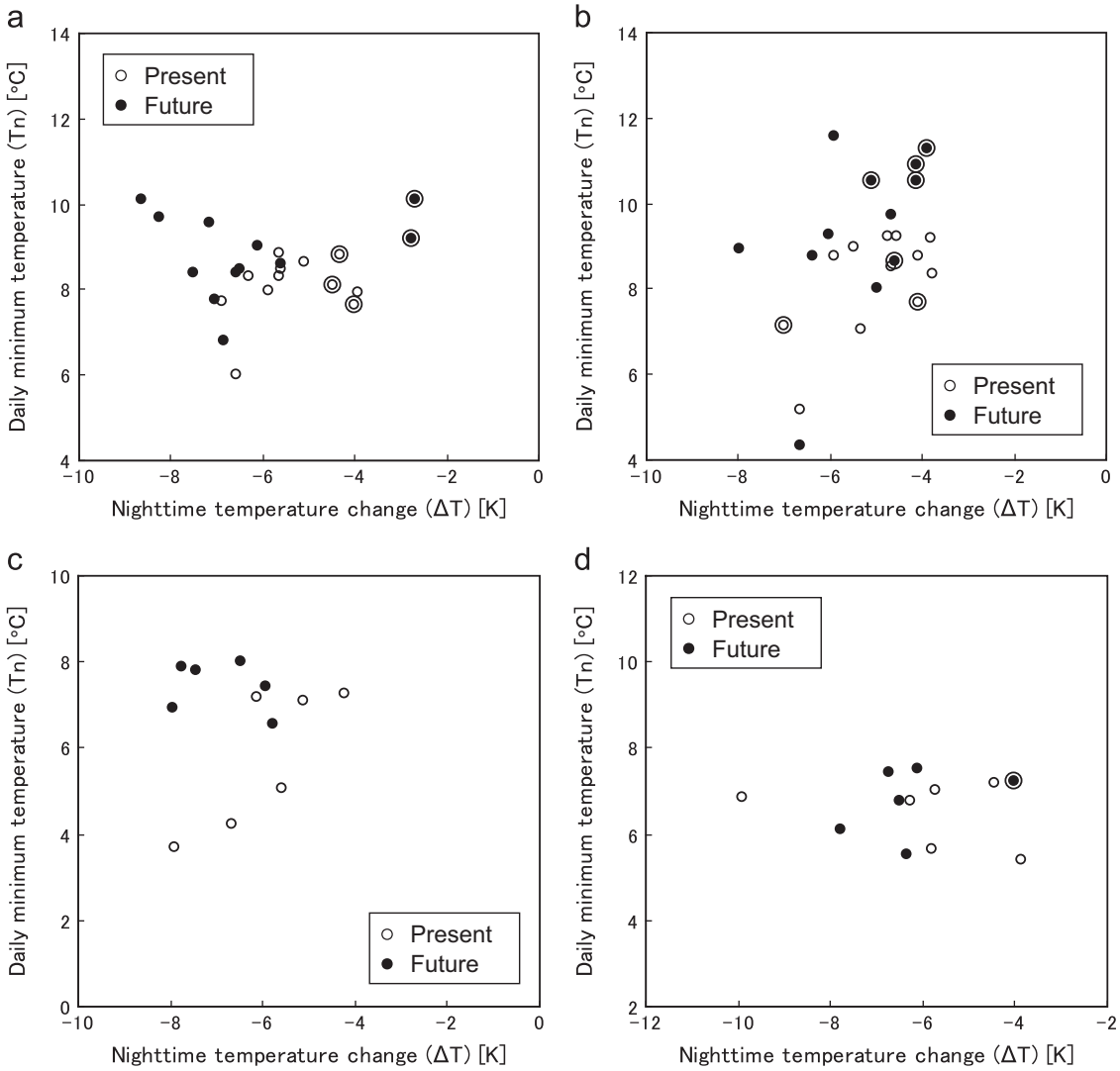

Fig. 5. As for Fig. 4, but for extremely-low daily minimum temperatures. The (a and b) 2% or (c and d) 1% of days with the coldest daily minimum temperatures are selected. Circles surrounding data marks denote 10 m wind speeds (averaged over the nighttime) greater than 2.2 m s^{-1}.

is accounted for by the total heat flux at the ground surface (Fig. 7a). Here the cases in which Tn is at or lower than Tn02 are selected and the cases in which surface wind speed is large (over 2.2 m s^{-1}) are excluded from this analysis. Although the ranges of ΔT and total heat flux overlaps considerably between the present and future climate, values of both tend to be lower in the future than in the present climate. The differences in both ΔT and the total heat flux between the present and future climates are statistically significant (Wilcoxon–Mann–Whitney rank-sum test (Wilks 2011) at the 5% level). These results suggest that the atmospheric situations for the two climates are quite different.

For the other three locations (i.e., Yusuhara, Kamioka, and Inabu), the relationship between the total heat flux and ΔT is similar to that at Kuma. That is, ΔT is roughly proportional to the total heat flux and values of both tend to be lower in the future climate than in the present climate (Fig. 7b–d). At Yusuhara and Kamioka, the differences in both ΔT and the total heat flux between the present and future climates are statistically significant (Wilcoxon–Mann–Whitney rank-sum test at the 5% level at Yusuhara and 10% level at Kamioka). At Inabu, on the other hand, the difference in the total heat flux between the two climates is not statistically significant, although the significance level of the difference in ΔT is 10%. Therefore, the data at Inabu are excluded from analyses described below.

We attribute the difference in the total heat flux at Kuma between the present and future climates to change in upward longwave radiation and latent heat flux. This result is achieved by performing a budget analysis of heat flux at the ground surface for each climate (Fig. 8) and by calculating the difference in heat flux between the two climates (Fig. 9a). The cases in which Tn is at or lower than Tn02 are used whereas the cases in which surface wind speed is over 2.2 m s^{-1} are excluded in the analysis. Note that positive (negative) is heat flux inward to (outward from) the surface that causes heating (cooling) of the surface. For example, upward longwave radiation shows negative (Fig. 8), indicating cooling at the surface due to outgoing longwave radiation. Moreover, the difference in upward longwave radiation between the two climates shows negative (Fig. 9), indicating that the cooling is greater in the future climate than in the present climate. We found that the differences in upward longwave radiation and latent heat flux contribute considerably to the total heat flux and that these two components relate similarly to the total heat flux (i.e., negative difference). In contrast, the differences in downward longwave radiation and heat flux under the ground are positive,

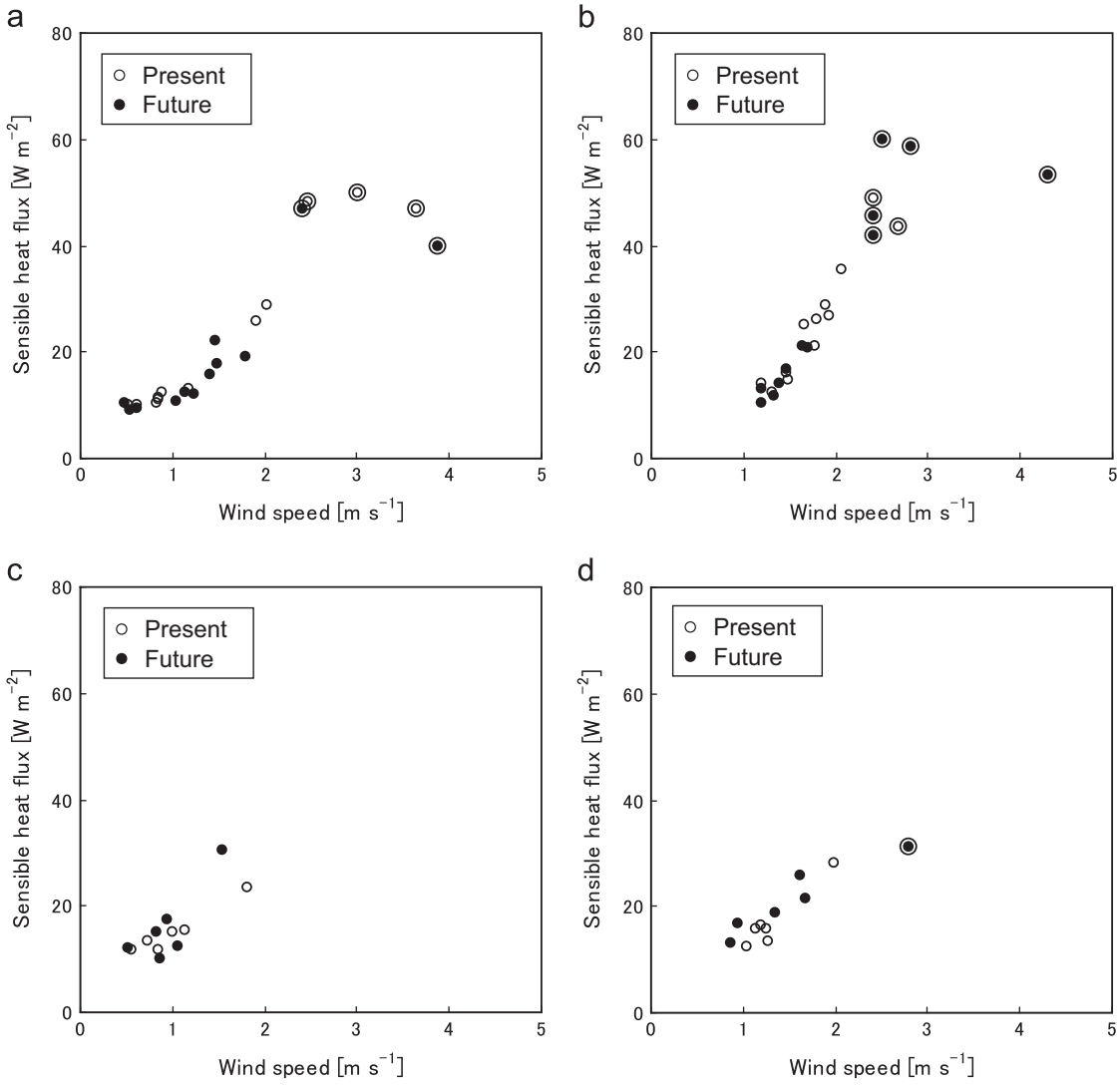

Fig. 6. As for Fig. 5, but downward sensible heat flux at the surface versus wind speed at 10 m. The heat flux and wind speed are averaged over the nighttime.

which are opposite to that of the total heat flux. The contribution of the difference in sensible heat flux to that in the total heat flux depends on locations.

For the other two locations (i.e., Yusuhara and Kamioka), the differences in the components of heat flux between the present and future climates are similar to those at Kuma. That is, upward longwave radiation and latent heat flux contribute to stronger cooling in the future climate (Fig. 9b and c). In addition, sensible heat flux contributes to the cooling at Yusuhara (Fig. 9b). We examined in detail these heat fluxes: upward longwave radiation, latent heat flux, and sensible heat flux.

5.2.1. *Upward longwave radiation*

Longwave radiative cooling is considered to be the dominant process for a large decrease in surface temperature on clear nights (e.g., Petty, 2004). In this situation, the cooling rate at the surface is approximately proportional to the magnitude of net radiation (outgoing longwave radiation from the surface minus incoming longwave radiation into the surface). The dominance of longwave radiation in the total heat flux holds true for the present cases in both the present and future climates (Fig. 8). The difference in longwave radiation between the present and future climates is important for the difference in the nighttime temperature drop between the two climates.

We attribute the difference in upward (outgoing) longwave radiation between the present and future climates to the temperature at the ground surface around the time of the sunset. At that time, the surface in the future climate is warmer than that in the present climate because of global warming (not shown). The warmer surface in the future climate is responsible for enhanced upward radiation as required by the Stefan–Boltzmann law, leading to more cooling at the surface compared with that in the present climate. The greater the cooling at the surface, the larger the temperature drop in the nighttime. Thus, upward longwave radiation acts to reduce the difference in the surface temperature between the two climates.

5.2.2. *Latent heat flux*

Dryer conditions just above the surface are responsible for enhanced upward (outgoing) latent heat flux in the future climate. Fig. 10 reveals that latent heat flux (negative is upward) roughly proportional to relative humidity at 16 m above the surface at all three locations. The values of latent heat flux and relative humidity tend to be lower in the future than in the present climate although the ranges of both overlaps considerably

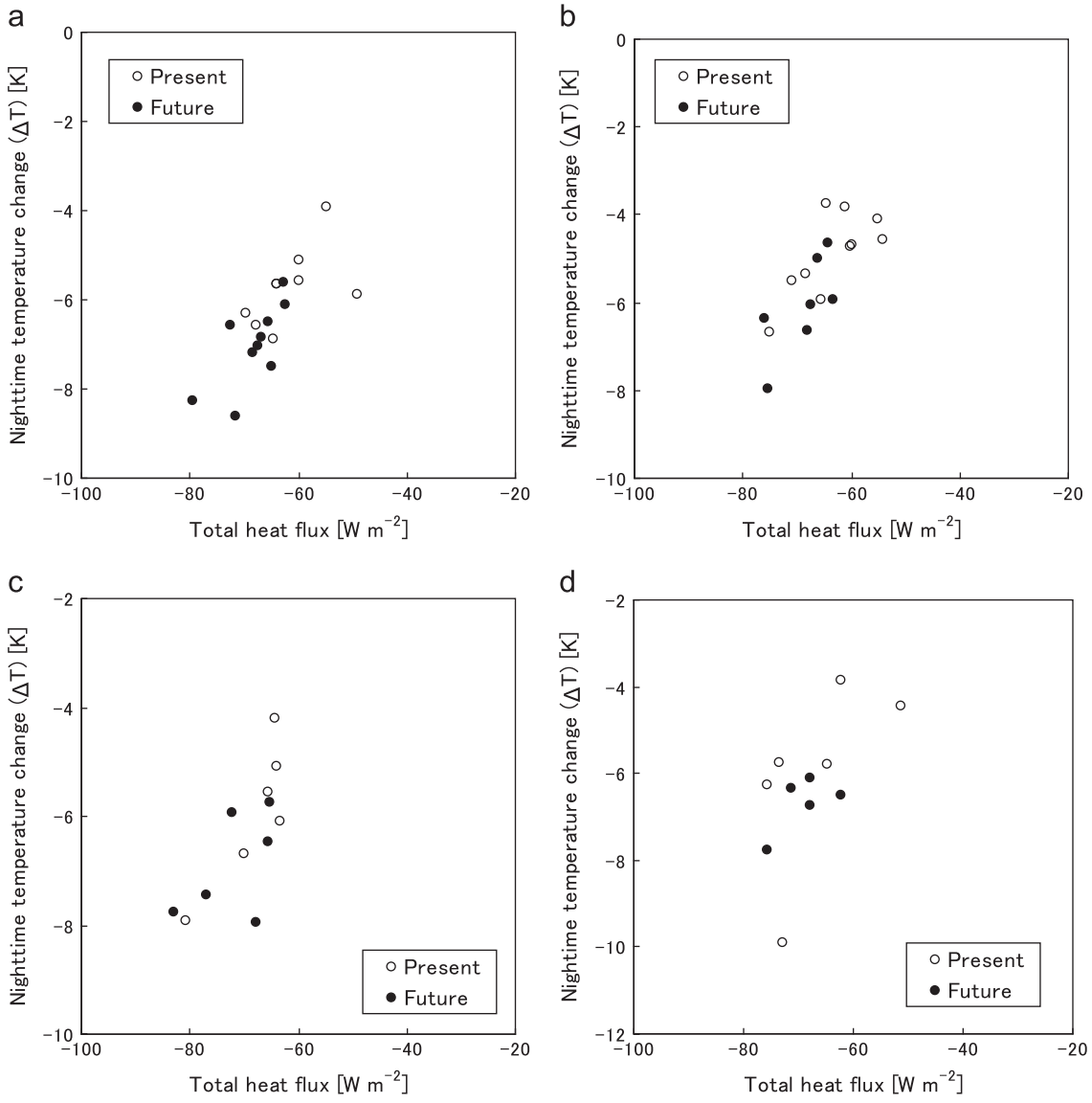

Fig. 7. As for Fig. 5, but change in daily surface air temperature at nighttime versus total heat flux at the surface (positive is downward). The heat flux are averaged over the nighttime. Data for surface wind speed over 2.2 m s^{-1} are excluded from the plot.

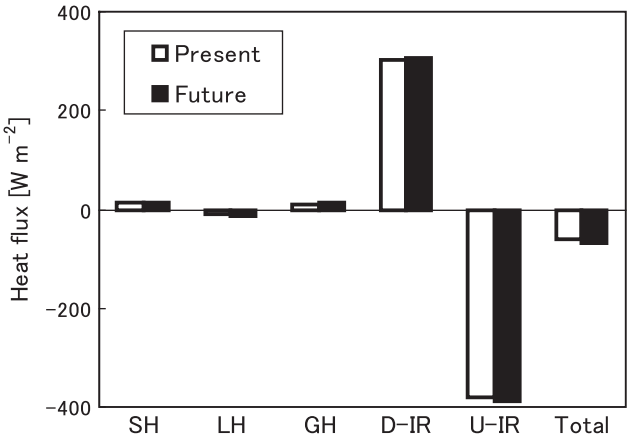

Fig. 8. Components of heat flux at the ground surface of Kuma in June for the present and future climate simulated by the NHRCM05. Positive values mean warming, whereas negative values mean cooling. Each component is averaged over the selected data, which are averaged over the nighttime, as shown in Fig. 7a.

between the present and future climates. The results indicate that dryer conditions just above the surface promote evaporative cooling at the surface (i.e., upward latent heat flux) in the future climate.

Dryer conditions near the surface are associated with atmospheric situations in the lower troposphere. Closer inspection of atmospheric moisture reveals that relative humidity at 16 m above the surface is roughly proportional to that at 850 hPa at all 3 locations although the values are varied more widely at a location (not shown). Relative humidity at 850 hPa tends to be lower in the future than in the present climate. This lower relative humidity at 850 hPa in the future climate suggests the influence of synoptic systems on the humidity. Further work on synoptic situations is required, which is beyond the scope of this study but will be the topic of future research.

It should be noted that the difference in latent heat flux between the present and future climates is not negligible compared with difference in other components of heat flux (Fig. 9) although the magnitude of latent heat flux is much smaller that those of radiation (Fig. 8). In addition, latent heat flux during the

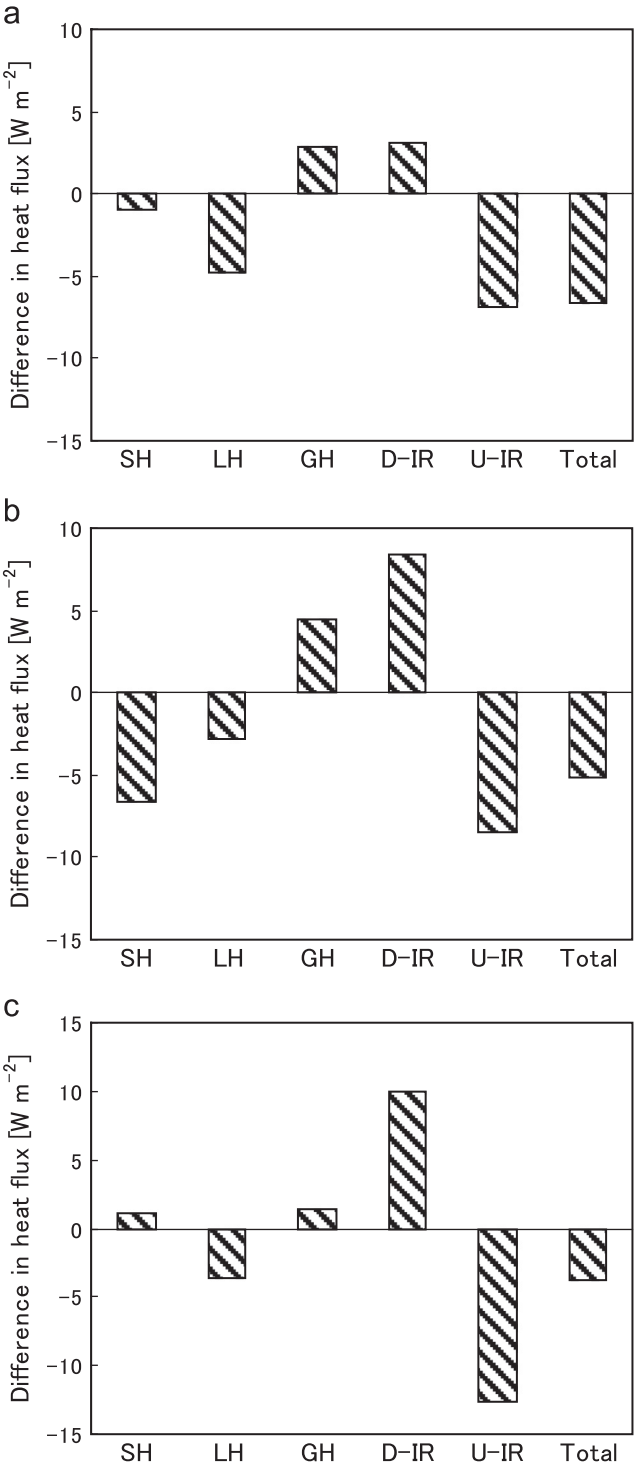

Fig. 9. Differences in components of heat flux between future and present climates (future minus present) simulated by the NHRCM05 for the surface at (a) Kuma, (b) Yusuhara, and (c) Kamioka, in June (SH: downward sensible heat flux, LH: downward latent heat flux, GH: upward heat flux from inside of the ground, D-IR: downward longwave radiation, U-IR: upward longwave radiation, Total: the sum of all components). Negative values mean more cooling or less warming in the future climate compared with the present climate. Each component is averaged over the selected data, which are averaged over the nighttime, as shown in Fig. 7.

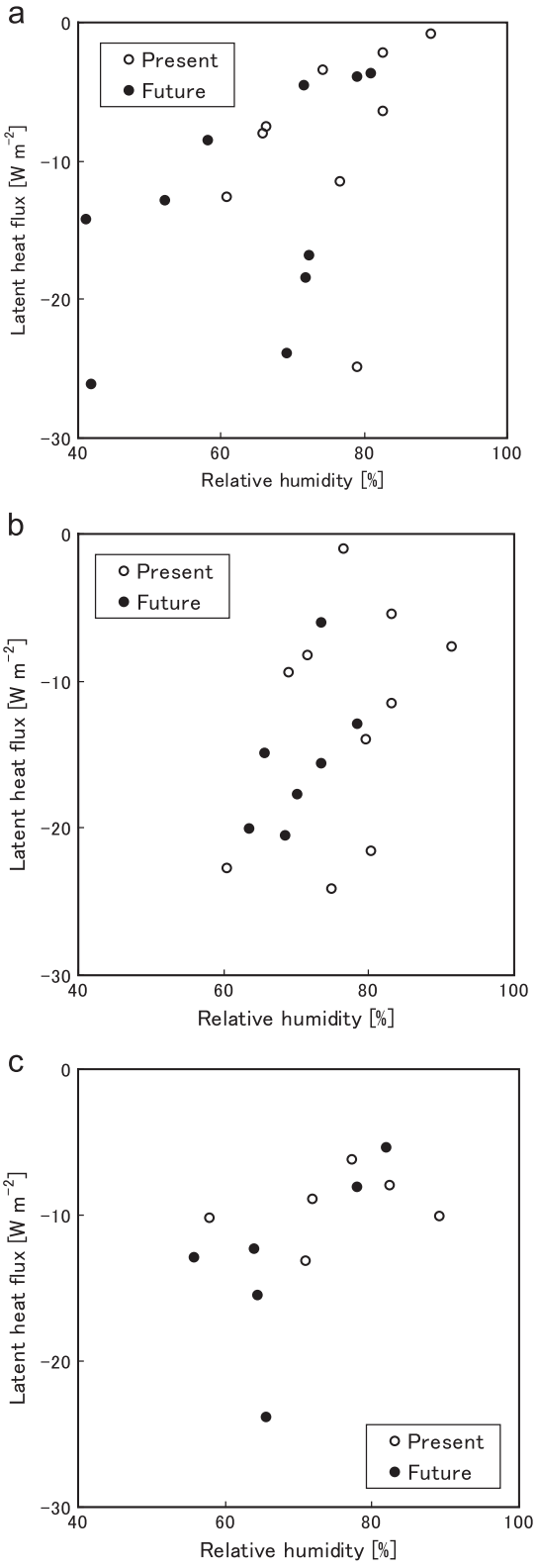

Fig. 10. Relative humidity 16 m above the surface versus downward latent heat flux (negative is upward) at the surface at (a) Kuma, (b) Yusuhara, and (c) Kamioka, in June for the present and future climate simulated by the NHRCM05. Relative humidity and latent heat flux are averaged over the nighttime.

nighttime is possible because the surface conditions are sufficiently wet and atmosphere just above the surface is dry. Soil moisture just below the surface is over 70% of the saturation in most cases (Fig. 11) and evaporative cooling tends to increase with drying atmosphere just above the surface (Fig. 10).

5.2.3. *Sensible heat flux*

The difference in sensible heat flux in the present and future climates is attributed to that in the surface wind speed. At Yusuhara, wind speed at 10 m in the future climate tends to be

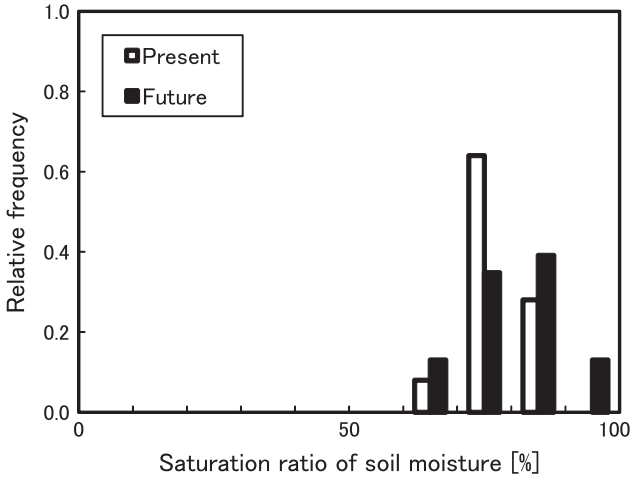

Fig. 11. Relative frequency of saturation ratio of soil moisture in the soil layer just below the surface. The saturation ratio is averaged over the nighttime. The selected data at Kuma, Yusuhara, and Kamioka, corresponding to those in Fig. 10, are used without differentiation between these locations.

smaller than that in the present climate, except for the excluded data (Fig. 6b). This result indicates that downward (incoming) sensible heat flux is not large in the future climate owing to less turbulent atmosphere. However, Kuma and Kamioka are not in similar situations. At these locations, there is no obvious difference in the surface wind speed between the two climates (Fig. 6a and c). Thus, the contribution of sensible heat flux to the total heat flux depends on the location.

6. Reliability measured by the bootstrap method

There are two approaches to reduce uncertainty in the estimates of climate change. One is to conduct ensemble simulations with RCMs that have a relatively low resolution. The other is to conduct a simulation with an RCM with higher resolution (e.g., Kendon et al., 2012). The approach adopted in this study is the latter. A well-developed high-resolution model provides a credible means to improve the performance of a model simulation with coarser resolution. As mentioned earlier, the horizontal grid spacing of the NHRCM05 is 5 km and is fine enough to resolve regional-scale and local-scale features, particularly involving interactions with complex topography. Moreover, simulation results produced by an operational model are more reliable because specific tuning of physical parameterizations is performed so as to obtain results suitable for a targeted region. Because the NHRCM05 is based on an operational model JMA-NHM, the NHRCM05 simulates the present climate well (Sasaki et al., 2011; Murata et al., 2013). The NHRCM05 simulations provide a credible means to obtain reliable estimates of temperature and other relevant features at least for the present climate but possibly for the future climate.

Uncertainties in projected future climates can be assessed by employing the bootstrapping approach even for results from a single-model simulation. The bootstrap is a kind of resampling procedure (Efron, 1979) and has been used for nonparametric testing. In such testing, the test statistic is calculated for each group of resampled data, and many groups of resampled data are prepared.

In this study, uncertainty about Tn01 at the three stations (i.e., Kuma, Yusuhara, and Kamioka) in June was assessed by means of the bootstrap approach. The procedure for assessing uncertainty at each station was as follows: (1) the simulated Tn in June was chosen for the present and future climates (600 data = 30 days × 20 years for each climate) and Tn01 was calculated; (2) to test under the null hypothesis that there is no significant difference in Tn01 between the two climates, the two dataset were merged (number of data points = 1200); (3) with the merged dataset, 10,000 resamplings were performed, and Tn01 for each resampled dataset was recalculated; and (4) the null hypothesis was tested by evaluating bootstrap realizations of the test statistic using the resampled datasets.

The results obtained by the bootstrap approach indicate that Tn01 in the future climate is comparable to that in the present climate at all three locations in June. The null hypothesis that there is no statistically significant difference in Tn01 between the two climates is not rejected at the 95% level of confidence at Kuma, and at the 99% level of confidence at Yusuhara and Kamioka. The results suggest that difference in Tn01 between the two climates at each location is not great.

7. Summary and concluding remarks

We examined mechanisms of early-summer low-temperature extremes in Japan at the end of the 21st century with projected temperature data provided by a well-developed high-resolution NHRCM05. The horizontal grid spacing of the NHRCM05 is 5 km so that it is possible to resolve the complex topography of Japan and the surface air temperatures influenced by topographic features. The NHRCM05 was driven at the lateral boundaries by GCM forcing under the A1B scenario provided by the IPCC-SRES.

First, we investigated the reproducibility of extremely low temperatures in June. The magnitudes of RMSE and the bias for Tn01 were approximately 2.2 K and 1.2 K, respectively, suggesting that the NHRCM05 has somewhat large errors in Tn01. After applying the bias correction proposed by Piani et al. (2010), errors in Tn01 in June showed much smaller values: the magnitudes of the RMSE and the bias were approximately 1.0 K and 0.4 K, respectively. The frequency distribution of Tn01 was also well reproduced by applying the bias correction.

Next, we investigated the projection of extremely low temperatures in June in the future climate. There were some locations where the changes in Tn01 were very small (below 1.0 K), suggesting that extremely low temperatures in the future climate would be comparable to those in the present climate.

We attribute the small Tn01 in the future climate to a relatively large drop in surface air temperature at nighttime. Budget analyses of surface energy reveal that the upward (outgoing) fluxes of longwave radiation and latent heat (i.e., evaporative cooling) are responsible for the small magnitude of the changes; specifically, in the future climate, both upward fluxes from the ground surface increase. This enhanced upward radiation in the future climate is caused by higher temperature at the surface around the time of the sunset. The increase in the upward flux of latent heat is caused by low relative humidity just above the surface in the future climate. The dryer conditions near the surface are associated with those at 850 hPa, suggesting the influence of synoptic systems. In conclusion, greater outgoing longwave radiation in the future climate, compared with the present climate, is mainly responsible for the extreme temperature drop at nighttime although the radiative cooling is the main process for both climates. In addition, evaporative cooling is needed to further reduce temperature in the future climate.

We demonstrated that, in the future climate, extremely low temperatures comparable to those in the present climate could occur in some locations. Our results could be generalized to the mechanism of extremely low temperatures over mountainous areas in Japan, although we focused on physical processes over mountainous locations (i.e., Kuma, Yusuhara, and Kamioka) in this

study. To support this hypothesis, further investigation similar to the present study is needed for other locations where the low temperatures in the future climate would be comparable to those in the present climate.

Acknowledgments

Numerical simulations obtained with AGCM20 were conducted under the framework of the "Projection of the change in future weather extremes using super-high-resolution atmospheric models" supported by the KAKUSHIN Program of the Ministry of Education, Culture, Sports, Science, and Technology in Japan. These simulations were performed on the Earth Simulator.

References

Anderson, B.T., 2011. Near-term increase in frequency of seasonal temperature extremes prior to the 2 °C global warming target. Clim. Change 108, 581–589, http://dx.doi.org/10.1007/s10584-011-0196-4.

Anderson, B.T., 2012. Intensification of seasonal extremes given a 2 °C global warming target. Clim. Change 112, 325–337, http://dx.doi.org/10.1007/s10584-011-0213-7.

Arritt, R.W., Rummukainen, M., 2011. Challenges in regional-scale climate modeling. Bull. Am. Meteorol. Soc. 92, 365–368, http://dx.doi.org/10.1175/2010BAMS2971.1.

Bai, Y., Kaneko, I., Kobayashi, H., Kurihara, K., Takayabu, I., Sasaki, H., Murata, A., 2013. A geographic information system (GIS)-based approach to adaptation to regional climate change: a case study of Okutama-machi, Tokyo, Japan. Mitig. Adapt. Strateg. Glob. Change , http://dx.doi.org/10.1007/s11027-013-9450-6.

Beljaars, A.C.M., Holtslag, A.A.M., 1991. Flux parameterization over land surfaces for atmospheric models. J. Appl. Meteorol. 30, 327–341.

Bordoy, R., Burlando, P., 2013. Bias correction of regional climate model simulations in a region of complex orography. J. Appl. Meteorol. Climatol. 52, 82–101, http://dx.doi.org/10.1175/JAMC-D-11-0149.1.

Bourke, R.H., Garrett, R.P., 1987. Sea ice thickness distribution in the Arctic ocean, cold regions. Sci. Technol. 13, 259–280, http://dx.doi.org/10.1016/0165-232X(87)90007-3.

Efron, B., 1979. Bootstrap methods: another look at the jackknife. Ann. Stat. 7, 1–26.

Frías, M.D., Minguez, R., Gutierrez, J.M., Mendez, F.J., 2012. Future regional projections of extreme temperatures in Europe: a nonstationary seasonal approach. Clim. Change 113, 371–392, http://dx.doi.org/10.1007/s10584-011-0351-y.

Hanafusa, M., Sasaki, H., Murata, A., Kurihara, K., 2013. Projection of changes in future surface wind around Japan using a non-hydrostatic regional climate model. SOLA 9, 23–26, http://dx.doi.org/10.2151/sola.2013-006.

Handmer, J., Honda, Y., Kundzewicz, Z.W., Arnell, N., Benito, G., Hatfield, J., Mohamed, I.F., Peduzzi, P., Wu, S., Sherstyukov, B., Takahashi, K., Yan, Z., 2012. Changes in impacts of climate extremes: human systems and ecosystems. In: Field, C.B., Barros, V., Stocker, T.F., Qin, D., Dokken, D.J., Ebi, K.L., Mastrandrea, M. D., Mach, K.J., Plattner, G.-K., Allen, S.K., Tignor, M., Midgley, P.M. (Eds.), Managing the Risks of Extreme Events and Disasters to Advance Climate Change Adaptation, A Special Report of Working Groups I and II of the Intergovernmental Panel on Climate Change (IPCC). Cambridge University Press, Cambridge, UK, and New York, NY, USA, pp. 231–290.

Hirai M., Ohizumi M., Development of a new land-surface model for JMA-GSM. Extended abstract of 20th Conference on Weather Analysis and Forecasting/16th Conference on NWP. P2.22 (Available at ⟨http://ams.confex.com/ams/84Annual/techprogram/paper_68652.htm⟩), 2004.

Hurkmans, R., Terink, W., Uijlenhoet, R., Torfs, P., Jacob, D., Troch, P.A., 2010. Changes in streamflow dynamics in the Rhine basin under three high-resolution regional climate scenarios. J. Clim. 23, 679–699, http://dx.doi.org/10.1175/2009JCLI3066.1.

IPCC (Intergovernmental Panel on Climate Change), 2000. Special report on emissions scenarios. In: Nakic'enovic', N., Alcamo, J., Davis, G., de Vries, B., Fenhann, J., Gaffin, S., Gregory, K., Grübler, A., Yong Jung, T., Kram, T., La Rovere, E.L., Michaelis, L., Mori, S., Morita, T., Pepper, W., Pitcher, H., Price, L., Riahi, K., Roehrl, A., Rogner, H.-H., Sankovski, A., Schlesinger, M., Shukla, P., Smith, S., Swart, R., van Rooijen, S., Victor, N., Dadi, Z. (Eds.), A Special Report of Working Group III of the Intergovernmental Panel on Climate Change. Cambridge University Press, Cambridge, UK, p. 595.

IPCC (Intergovernmental Panel on Climate Change), 2007. Climate change: the physical science basis. In: Solomon, S., Qin, D., Manning, M., Chen, Z., Marquis, M., Averyt, K.B., Tignor, M., Miller, H.L. (Eds.), Contribution of Working Group I to the Fourth Assessment Report of the Intergovernmental Panel on Climate Change. Cambridge University Press, Cambridge, UK and New York, NY, USA, p. 996.

Ikawa, M., Mizuno, H., Matsuo, T., Murakami, M., Yamada, Y., Saito, K., 1991. Numerical modeling of the convective snow cloud over the Sea of Japan. Precipitation mechanism and sensitivity to ice crystal nucleation rates. J. Meteorol. Soc. Jpn. 69, 641–667.

Inouye, D.W., 2000. The ecological and evolutionary significance of frost in the context of climate change. Ecol. Lett. 3, 457–463.

Kain, J.S., 2004. The Kain–Fritsch, convective parameterization: an update. J. Appl. Meteorol. 43, 170–181.

Kain, J.S., Fritsch, J.M., 1990. A one-dimensional entrainment/detrainment plume model and its application in convective parameterization. J. Atmos. Sci. 47, 2784–2802.

Kanada, S., Nakano, M., Hayashi, S., Kato, T., Nakamura, M., Kurihara, K., 2008. Reproducibility of maximum daily precipitation amount over Japan by a high resolution non-hydrostatic model. SOLA 4, 105–108, http://dx.doi.org/10.2151/sola.2008-027.

Kato, T., Yamada, Y., Nakano, M., 2010. Improvement of Kain–Fritsch convection parameterization scheme to suppress its false predictions of rainfall areas along coastal lines. CAS/JSC WGNE Res. Act. Atmos. Ocean. Model. 40, 4.07–4.08.

Kendon, E.J., Roberts, N.M., Senior, C.A., Roberts, M.J., 2012. Realism of rainfall in a very high-resolution regional climate model. J. Clim. 25, 5791–5806, http://dx.doi.org/10.1175/JCLI-D-11-00562.1.

Kida, H., Koide, T., Sasaki, H., Chiba, M., 1991. A new approach to coupling a limited area model with a GCM for regional climate simulations. J. Meteorol. Soc. Jpn. 69, 723–728.

Kitagawa, H., 2000. Radiation processes. Sep. Vol. Annu. Rep. NPD 46, 16–31 (in Japanese).

Kitoh, A., Ose, T., Kurihara, K., Kusunoki, S., Sugi, M., 2009. KAKUSHIN Team-3 modeling group, projection of changes in future weather extremes using super-high-resolution global and regional atmospheric models in the KAKUSHIN program: results of preliminary experiments. Hydrol. Res. Lett. 3, 49–53, http://dx.doi.org/10.3178/HRL.3.49.

Kodra, E., Steinhaeuser, K., Ganguly, A.R., 2011. Persisting cold extremes under 21st century warming scenarios. Geophys. Res. Lett. 38, L08705, http://dx.doi.org/10.1029/2011GL047103.

Kurihara, K., Ishihara, K., Sasaki, H., Fukuyama, Y., Saitou, H., Takayabu, I., Murazaki, K., Sato, Y., Yukimoto, S., Noda, A., 2005. Projection of climatic change over Japan due to global warming by high resolution regional climate model in MRI. SOLA 1, 97–100, http://dx.doi.org/10.2151/sola.2005-026.

Leander, R., Buishand, T.A., 2007. Resampling of regional climate model output for the simulation of extreme river flows. J. Hydrol. 332, 487–496, http://dx.doi.org/10.1016/j.jhydrol.2006.08.006.

Lin, Y.H., Farley, R.D., Orville, H.D., 1983. Bulk parameterization of the snow field in a cloud model. J. Clim. Appl. Meteorol. 22, 1065–1092.

Luo, Q., 2011. Temperature thresholds and crop production: a review. Clim. Change 109, 583–598, http://dx.doi.org/10.1007/s10584-011-0028-6.

Mizuta, R., Yoshimura, H., Murakami, H., Matsueda, M., Endo, H., Ose, T., Kamiguchi, K., Hosaka, M., Sugi, M., Yukimoto, S., Kusunoki, S., Kitoh, A., 2012. Climate simulations using the improved MRI-AGCM with 20-km grid. J. Meteorol. Soc. Jpn. 90A, 233–258.

Murakami, M., 1990. Numerical modeling of dynamical and microphysical evolution of an isolated convective cloud. The 19 July 1981 CCOPE cloud -. J. Meteorol. Soc. Jpn. 68, 107–128.

Murakami, M., Clark, T.L., Hall, W.D., 1994. Numerical simulation of convective snow clouds over the Sea of Japan; two-dimensional simulation of mixed layer development and convective snow cloud formation. J. Meteorol. Soc. Jpn. 72, 43–62.

Murata, A., Nakano, M., Kanada, S., Kurihara, K., Sasaki, H., 2012. Summertime temperature extremes over Japan in the late 21st century projected by a high-resolution regional climate model. J. Meteorol. Soc. Jpn. 90A, 101–122.

Murata, A., Sasaki, H., Hanafusa, M., Kurihara, K., 2013. Estimation of urban heat island intensity using biases in surface air temperature simulated by a nonhydrostatic regional climate model. Theor. Appl. Climatol. 112, 351–361, http://dx.doi.org/10.1007/s00704-012-0739-2.

Nakanishi, M., Niino, H., 2004. An improved Mellor–Yamada level-3 model with condensation physics: its design and verification. Bound. Layer Meteor 112, 1–31.

Nakano, M., Kato, T., Hayashi, S., Kanada, S., Yamada, Y., Kurihara, K., 2012. Development of a 5-km-mesh cloud-system-resolving regional climate model at the Meteorological Research Institute. J. Meteorol. Soc. Jpn. 90A, 339–350.

Park, T.-W., Ho, C.-H., Jeong, S.-J., Choi, Y.-S., Park, S.K., Song, C.-K., 2011. Different characteristics of cold day and cold surge frequency over East Asia in a global warming situation. J. Geophys. Res. 116, D12118, http://dx.doi.org/10.29/2010JD015369.

Patz, J.A., Campbell-Lendrum, D., Holloway, T., Foley, J.A., 2005. Impact of regional climate change on human health. Nature 438, 310–317, http://dx.doi.org/10.1038/nature04188.

Petty, G.W., 2004. A First Course of Atmospheric Radiation. Sundog Publication, Madison, Wisconsin.

Piani, C., Haerter, J.O., Coppola, E., 2010a. Statistical bias correction for daily precipitation in regional climate models over Europe. Theor. Appl. Climatol. 99, 187–192, http://dx.doi.org/10.1007/s00704-009-0134-9.

Piani, C., Weedon, G.P., Best, M., Gomes, S.M., Viterbo, P., Hagemann, S., Haerter, J.O., 2010b. Statistical bias correction of global simulated daily precipitation and temperature for the application of hydrological models. J. Hydrol. 395, 199–215, http://dx.doi.org/10.1016/j.jhydrol.2010.10.024.

Rangwala, I., Barsugli, J., Cozzetto, K., Neff, J., Prairie, J., 2012. Mid-21st century projections in temperature extremes in the southern Colorado Rocky Mountains from regional climate models. Clim. Dyn. 39, 1823–1840, http://dx.doi.org/10.1007/s00382-011-1282-z.

Rayner, N.A., Parker, D.E., Horton, E.B., Folland, C.K., Alexander, L.V., Rowell, D.P., Kent, E.C., Kaplan, A., 2003. Global analyses of sea surface temperature, sea ice, and night marine air temperature since the late nineteenth century. J. Geophys. Res. 108, D4407, http://dx.doi.org/10.1029/2002JD002670.

Rummukainen, M., 2010. State-of-the-art with regional climate models. WIREs Clim. Change 1, 82–96, http://dx.doi.org/10.1002/wcc.008.

Saito, K., Fujita, T., Yamada, Y., Ishida, J., Kumagai, Y., Aranami, K., Ohmori, S., Nagasawa, R., Kumagai, S., Muroi, C., Kato, T., Eito, H., Yamazaki, Y., 2006. The operational JMA nonhydrostatic mesoscale model. Mon. Weather Rev. 134, 1266–1298.

Saito, K., Ishida, J., Aranami, K., Hara, T., Segawa, T., Narita, M., Honda, Y., 2007. Nonhydrostatic atmospheric models and operational development at JMA. J. Meteorol. Soc. Jpn. 85B, 271–304.

Sasaki, H., Sato, Y., Adachi, K., Kida, H., 2000. Performance and evaluation of the MRI regional climate model with the spectral boundary coupling method. J. Meteorol. Soc. Jpn. 78, 477–489.

Sasaki, H., Kurihara, K., Takayabu, I., Uchiyama, T., 2008. Preliminary experiments of reproducing the present climate using the non-hydrostatic regional climate model. SOLA 4, 25–28, http://dx.doi.org/10.2151/sola.2008-007.

Sasaki, H., Murata, A., Hanafusa, M., Oh'izumi, M., Kurihara, K., 2011. Reproducibility of present climate in a non-hydrostatic regional climate model nested within an atmosphere general circulation model. SOLA 7, 173–176, http://dx.doi.org/10.2151/sola.2011-044.

Sasaki, H., Murata, A., Hanafusa, M., Oh'izumi, M., Kurihara, K., 2012. Projection of future climate change in a non-hydrostatic regional climate model nested within an atmospheric general circulation model. SOLA 8, 53–56, http://dx.doi.org/10.2151/sola.2012-014.

Sasaki, H., Kurihara, K., Murata, A., Hanafusa, M., Oh'izumi, M., 2013. Future changes of snow depth in a non-hydrostatic regional climate model with bias correction. SOLA 9, 5–8, http://dx.doi.org/10.2151/sola.2013-002.

Sellers, P.J., Mints, Y., Sud, Y.C., Dalcher, A., 1986. A Simple biosphere model (SiB) for use within general circulation models. J. Atmos. Sci. 43, 505–531.

Wilks, D.S., 2011. Statistical Methods in the Atmospheric Sciences, third ed. Academic Press, Oxford, UK.

Yabu, S., Murai, S., Kitagawa, H., 2005. Clear sky radiation scheme. Sep. Vol. Annu. Rep. NPD 51, 53–64 (in Japanese).